Physica Scripta Vol. T60, 81–90, 1995

Theory of Shear Alfvén Waves in Toroidal Plasmas

Liu Chen[1] and Fulvio Zonca[2]

[1]Department of Physics and Astronomy, University of California, Irvine, CA 92717-4575, U.S.A.
[2]Associazione EURATOM-ENEA sulla Fusione, C.P. 65-00044 Frascati, Rome, Italy

Received 21 July 1995; accepted 31 July 1995

Abstract

Fundamental wave and stability properties of shear Alfvén waves in nonuniform axisymmetric toroidal plasmas are reviewed. Using a slab model with nonuniform density, concepts such as continuous spectrum, resonant absorption, and linear mode conversion to kinetic Alfvén wave are first discussed. We then analyze the formation of frequency gaps in the continuous spectrum due to the finite toroidicity-induced coupling between the poloidal harmonics in an axisymmetric torus. Existence of discrete eigenmodes both inside the frequency gap and the continuous spectra are further demonstrated. Kinetic excitations of collective toroidal shear Alfvén instabilities via resonances with energetic particles are also reviewed; first in the one-dimensional radially local limit and then with a full two-dimensional global analysis. Effects due to the non-perturbative nature of the energetic-particle drive and the global extent of the eigenmodes are emphasized.

1. Introduction

Since first discovered by the late Professor Hannes Alfvén [1], magnetohydrodynamic (MHD) or Alfvén waves have been of fundamental importance to the dynamics of magnetized plasmas in both laboratory experiments and space environments. As the present review has an emphasis on the plasma stability properties, we shall focus on the shear Alfvén wave (SAW). This is because while the compressioned Alfvén and slow sound waves tend to be stabilized by the finite magnetic and/or plasma compression as well as finite ion Landau damping, SAW is nearly incompressible and, thus, most interesting at least from the stability point of view.

Briefly summarizing, SAW has parallel wavelengths, $\lambda_\parallel$, comparable to the system size along the equilibrium magnetic field. It can, however, have a wide range in the perpendicular wavelengths $\lambda_\perp$, $\rho_i < \lambda_\perp < L_\perp$; where ρ_i and $L_\perp$ are, respectively, the ion Larmor radius and system size perpendicular to $\boldsymbol{B}_0$. SAW, meanwhile, has frequencies $\omega \simeq k_\parallel V_A \sim O(V_A/L_\parallel)$ much less than the ion cyclotron frequency Ω_i. Here, $V_A = B_0/(4\pi n_0 m_i)^{1/2}$ is the Alfvén speed. SAW dynamics is, hence, of low-frequency and macroscopic scales and, therefore, may cause significant perturbations in the bulk of plasmas. This is one of the primary reasons why shear Alfvén waves play many important roles in laboratory and space plasmas. Some examples are (1) heating of laboratory [2, 3] and solar corona plasmas [4]; (2) resonant interactions with energetic ions produced during high-power neutral-beam and/or radio-frequency laboratory heating experiments or with alpha particles produced in deuterium-tritium fusion plasmas [5–7]; (3) cross-field transport in magnetospheric plasmas; e.g., the dayside magnetopause [8]; and (4) acceleration of electrons along the auroral field lines [9].

One of the unique and most important properties of SAW is that its group velocity $\boldsymbol{V}_g$ is confined along $\boldsymbol{B}_0$; i.e., $\boldsymbol{V}_g \simeq \boldsymbol{V}_A$. In nonuniform plasmas with spatially varying V_A this property can then lead to singular oscillations at local SAW frequency; since the wave energy will be confined to the local field line. As the local SAW frequency varies continuously, we then have oscillations which constitute the so-called shear Alfvén continuous spectrum or SAW continuum [10]. The existence of SAW continuum then suggests that at the layer where the frequency of the applied radio-frequency source matches the local SAW frequency, the wave equation has a singular turning point; leading to resonant wave absorption and the Alfvén wave heating scheme [2, 3]. That the wave solution becomes singular is, of course, due to the inadequacy of ideal MHD approximation. Including microscopic kinetic effects such as finite ion Larmor radii removes the singular behaviors by allowing small but finite $\boldsymbol{V}_g$ cross $\boldsymbol{B}_0$. That is, we have the linear mode conversion of resonant SAW to the kinetic Alfvén wave (KAW) [5, 11, 12]. These fundamental concepts and processes of SAW in *nonuniform* magnetized plasmas are reviewed in Section 2 using a simple slab model.

Section 3 reviews SAW in toroidal plasmas such as tokamaks. In contrast to cylindrical plasmas, equilibrium properties in tokamaks have poloidal dependencies due to the finite toroidicity; i.e., $\varepsilon \equiv a/R_0 \neq 0$. Here, a and R_0 are, respectively, the minor and major radii. Consequently, there is finite coupling between the neighboring poloidal dynamics. This finite-toroidicity coupling, in particular, modifies qualitatively the SAW continuum of the individual poloidal harmonics. Specifically, there appear frequency gaps in the SAW continuum around characteristic frequencies at which the SAW frequencies of the neighboring poloidal harmonics match [13]. One important discovery [14] is that discrete marginally stable eigenmodes, including the well-known toroidal Alfvén eigenmode (TAE) can exist within the frequency gaps. In addition, around the frequency gaps, resistive and/or kinetic Alfvén waves (KAW) can discretize the SAW continuum to form the so-called kinetic TAE (KTAE) [14, 15].

In current and future tokamak experiments with reactor-grade plasmas, there is, inevitably, presence of highly energetic ions produced by either high-power neutral-beam and/or radio-frequency heating and/or deuterium-tritium fusion reactions. Since the energetic ions have, typically, speeds comparable to V_A, one is straightforwardly led to investigate the excitations of collective instabilities via resonant interactions between discrete shear Alfvén waves and energetic ions and/or α particles. Section 4 contains a review of kinetic excitations of toroidal shear Alfvén modes in the radially local (i.e., only one dimension along $\boldsymbol{B}_0$) approximation [6, 16]. Adopting the generalized ballooning-mode formalism [17, 18], the stability analyses are further extended in Section 5 to two-dimensional global eigenmodes such that effects of radial equilibrium

profiles on the eigenmode stability and structure can be properly assessed [19].

Finally, Section 6 contains a brief summary and discussions of possible future research areas.

2. Shear Alfvén waves in a nonuniform slab plasma

The purpose of this Section is to review fundamental properties of SAW in nonuniform magnetized plasmas such as continuous spectrum, resonant absorption and mode conversion to kinetic Alfvén Wave (KAW).

Let us consider a magnetized plasma whose density depends on x; i.e., $n_0 = n_0(x)$ for $-\infty < x < \infty$. Meanwhile, $\boldsymbol{B}_0 = B_0 \boldsymbol{e}_z$ and the plasma is confined by two perfectly conducting plates at $z = 0$ and L. Adopting the ideal MHD approximation and assuming the plasma is cold, we obtain the following set of equations for the fluid displacement vector $\delta\boldsymbol{\xi}_\perp$;

$$D_A \delta\boldsymbol{\xi}_\perp = \boldsymbol{\nabla}_\perp (\delta B_\parallel / B_0), \tag{1}$$

$$\delta B_\parallel / B_0 = \boldsymbol{\nabla} \cdot \delta\boldsymbol{\xi}_\perp. \tag{2}$$

Here,

$$D_A = \frac{\partial^2}{\partial z^2} + \frac{\omega^2}{V_A^2(x)} \tag{3}$$

is the local SAW operator, $\delta B_\parallel = \delta\boldsymbol{B} \cdot \boldsymbol{B}_0 / B_0$ is the compressional component of the magnetic perturbation, $\boldsymbol{\nabla}_\perp = \boldsymbol{e}_y i k_y + \boldsymbol{e}_x \frac{\partial}{\partial x}$, and $\exp(-i\omega t + i k_y y)$ dependence is assumed. Equations (1) and (2) can be combined, in the form of operators, as

$$\left[\frac{\partial}{\partial x} \frac{D_A}{k_y^2 - D_A} \frac{\partial}{\partial x} - D_A \right] \delta\xi_x(x, z) = 0. \tag{4}$$

Note that in *uniform* plasmas, $\partial D_A / \partial x = 0$ and Eq. (4) reduces to $D_A \delta\xi_x = 0$ and $(\partial^2/\partial x^2 - k_y^2 + D_A)\delta\xi_x = 0$; i.e., uncoupled shear and compressional Alfvén waves, respectively. Equation (4), thus, demonstrates that, in *nonuniform* plasmas, $\partial D_A / \partial x \neq 0$ and two branches of Alfvén waves are coupled. As will be further substantiated in later discussions, we are interested in SAW with $k_y^2 \gg |D_A|$. Equation (4) then becomes [2]

$$\left[\frac{\partial}{\partial x} D_A \frac{\partial}{\partial x} - k_y^2 D_A \right] \delta\xi_x(x, z) = 0; \tag{5}$$

i.e., the compressional Alfvén wave becomes evanescent in this limit.

Equation (5) indicates that $\delta\xi_x$ may become singular as D_A vanishes. To examine the possible singular behaviors in more details, we define $\phi_n(z|x)$ and $\omega_{An}(x)$ as the (local) SAW eigenfunction and eigenfrequency, respectively. That is, we have for $n = 1, 2, 3 \ldots$

$$\left[\frac{\partial^2}{\partial z^2} + \frac{\omega_{An}^2(x)}{V_A^2(x)} \right] \phi_n(z|x) = 0; \tag{6}$$

subject to the boundary condition $\phi_n = 0$ at $z = 0, L$. Since the operator is self-adjoint in Eq. (6), ω_{An}^2 is real and ϕ_n forms an orthonormal complete set, that is, $\int_0^L dz\, V_A^2 \phi_n \phi_m = \delta_{n,m}$. In the present model, $\phi_n(z|x) = (1/V_A)(2/L)^{1/2} \sin k_n z$, $k_n = n\pi/L$ and $\omega_{An}^2(x) = k_n^2 V_A^2(x) \ldots \delta\xi_x$ can then be expressed as

$$\delta\xi_x = \sum_{n=1} \hat{\xi}_{xn}(x_0, x_1) \phi_n(z|x_1); \tag{7}$$

where, anticipating singular behaviors, we have introduced x_0 and x_1 as, respectively, fast (local singular) and slow (global equilibrium) radial variables. Equation (8) then becomes, in the lowest order,

$$\left[\frac{d}{dx_0} \varepsilon_{An} \frac{d}{dx_0} - k_y^2 \varepsilon_{An} \right] \hat{\xi}_{nx0} = 0; \tag{8}$$

where $\varepsilon_{An} = \omega^2 - \omega_{An}^2(x)$. Singular solutions then exist near $x = x_{nr}$ where $\omega^2 = \omega_{An}^2(x_{nr})$. Defining $x_0 \equiv x - x_{nr}$ and hence, $\varepsilon_{An} = \varepsilon'_{An} x_0$, Eq. (8) can be readily solved to yield

$$\hat{\xi}_{nx0} = \frac{C_1(x_1)}{\varepsilon'_{An}} \ln(x - x_{nn}). \tag{9}$$

Here, only the singular solution of interest is presented. From the corresponding x-component of Eq. (1), one can readily show that, for $\delta B_\parallel = \sum_n \hat{B}_n \phi_n$, $\hat{B}_n$ is, in the lowest order, independent of x_0; i.e., $\hat{B}_n \simeq \hat{B}_{n0}(x_1)$. Meanwhile, from Eq. (2), one readily finds $\boldsymbol{\nabla}_\perp \cdot \hat{\boldsymbol{\xi}}_{n0} = 0$; i.e.,

$$\hat{\xi}_{ny0} = i C_n(x_1) / [k_y \varepsilon'_{An}(x - x_{nr})]. \tag{10}$$

Note that the coefficient of the singular solution C_n is intrinsically related to $\hat{B}_{n0}$ via the y-component of Eq. (1);

$$C_n = k_y^2 \hat{B}_{n0} / B_0. \tag{11}$$

Equation (11) further indicates that, in nonuniform plasmas, the singular solutions occur due to the finite coupling between the compressional Alfvén wave and the local SAW oscillations at $\omega = \omega_{An}(x) = k_n V_A(x)$. Since $\omega_{An}(x)$ varies continuously in x, local shear Alfvén oscillations therefore form a continuous spectrum or SAW continuum.

That the solution is singular further indicates that, in the steady state, the wave energy carried by the compressional Alfvén wave is piling up at $x = x_{nr}$; i.e., the shear Alfvén wave resonance layer. In other words, a finite amount of the wave energy can be resonantly absorbed at the SAW resonance layer and this leads to suggestions [2, 3] of localized heating schemes for both laboratory and solar corona plasmas [4]. Specifically, the resonant energy absorption rate is given by [2]

$$\frac{dW}{dt} = (1/2)\Re L_y \int_0^L dz \int_{-\infty}^{\infty} dx\, \delta\boldsymbol{J} \cdot \delta\boldsymbol{E}^*$$

$$= (\omega_0 / 8\pi) B_0 L_y \int_0^L dz \int_{-\infty}^{\infty} dx\, \Im[\delta\xi_x^* \partial \delta B_\parallel / \partial x].$$

Noting that the absorption is highly localized around $x = x_{nr}$ and $\Im\omega > 0$ from the causality constraint, we have

$$\frac{dW}{dt} = (\omega_0 / 8\pi) L_y |k_y \hat{B}_{n0} / V_A|^2 / |\varepsilon'_{An}|. \tag{12}$$

Here, the expressions are evaluated at $x = x_{nr}$. Note that, characteristic of resonant absorption, the absorption rate is independent of the detailed dissipation mechanisms.

While it has been shown that the steady-state solution is singular, it remains instructive to examine the asymptotic finite-time responses to initial perturbations. Anticipating that, as $t \to \infty$, $|\partial/\partial x| \to |\partial/\partial x_0| \gg |k_y|$, Eq. (8) becomes, correspondingly,

$$\frac{\partial}{\partial x_0} \left[\frac{\partial^2}{\partial t^2} + \omega_{An}^2(x) \right] \frac{\partial}{\partial x_0} \hat{\xi}_{nx}(x_0, t) = 0. \tag{13}$$

One then readily derives

$$\xi_{nx}(x_0, t) = \mp i \frac{C_n(x_1)}{\omega'_{An} t} \exp[\pm i \omega_{An}(x_1) t], \tag{14}$$

and

$$\hat{\xi}_{ny}(x_0, t) = (i/k_y) C_n(x_1) \exp[\pm i \omega_{An}(x_1) t]. \tag{15}$$

Equation (15) clearly shows the undamped oscillations of $\hat{\xi}_{ny}$ at frequencies corresponding to the SAW continuum. $\hat{\xi}_{nx}$, meanwhile, suffers $1/t$ decay due to the phase mixing of SAW continuum. Equations (14) and (15) suggest an effective wavenumber

$$k_x \equiv |\partial/\partial x_0| = |\omega'_{An} t|, \tag{16}$$

and, hence, $k_x \to \infty$ as $t \to \infty$; which is consistent with the earlier observation that the solution becomes singular in the steady state.

That the solution is singular is a manifestation of the breakdown of ideal MHD approximation. By incorporating kinetic effects due to short perpendicular wavelengths such as finite ion Larmor radius and electron inertia, one removes the singularity by allowing the wave energy propagate across $\boldsymbol{B}_0$. The corresponding kinetic Alfvén wave (KAW) equation is

$$[\omega^2 \nabla_\perp^2 \hat{\rho}_K^2 \nabla_\perp^2 + \boldsymbol{\nabla}_\perp \cdot \varepsilon_{An} \boldsymbol{\nabla}_\perp] \delta\hat{\xi}_{xn} = 0, \tag{17}$$

where

$$\hat{\rho}_K^2 = \rho_i^2 \left[\frac{3}{4}(1 - i\delta_e) + \frac{T_e}{T_i}(1 - i\delta_e) \right], \tag{18}$$

δ_i and δ_e are, respectively, ion and electron dissipations, and $m_e/m_i \ll \beta_e \ll 1$ is assumed. Equation (17) clearly shows that, by introducing the additional $\hat{\rho}_K^2 \nabla_\perp^4$ term, the singularity at $\varepsilon_{An} = 0$ is removed. In fact, Eq. (17) describes the linear mode conversion of (cut-off) compressional Alfvén wave to the so-called kinetic Alfvén wave (KAW) around $\varepsilon_{An} = 0$ [11, 12]. In the WKB limit, the KAW dispersion relation is given by

$$\omega^2 = \omega_{An}^2(x)(1 + k_x^2 \hat{\rho}_K^2); \tag{19}$$

which shows that KAW is propagating (cut-off) for $\omega^2 > (<) \omega_{An}^2(x)$ or $\varepsilon_{An} > (<) 0$.

3. Shear Alfvén waves in toroidal plasmas

We consider an axisymmetric tokamak plasma with large aspect ratio $\varepsilon \equiv a/R \ll 1$ and shifted circular magnetic surfaces. Adopting r, χ, and ξ as, respectively, the radial, poloidal-angle and toroidal-angle coordinates, the perturbed field variable can be expressed as

$$\delta\phi(r, \chi, \xi, t) = \exp(-i\omega t + in\xi) \sum_m \delta\phi(r, m) \exp(-im\chi). \tag{20}$$

Here, n and m are toroidal and poloidal mode numbers, respectively. Note that because of finite ε, tokamak equilibria depend on χ and, hence, there is small but finite coupling among the poloidal harmonics, $\delta\phi(r, m)$.

For each $\delta\phi(r, m)$, the shear Alfvén wave frequency is given by $\omega_m^2 = [nq(r) - m]^2 \omega_A^2$. Here, $\omega_A = V_A/qR$ and q is the safety factor. As will be demonstrated in Section 4, collective Alfvén instabilities are excited by tapping the free energy of finite ion/alpha-particle pressure gradient, but damped by the stabilizing velocity gradient. It, hence, suggests that the most unstable modes tend to maximize $\omega_{*E} \propto n$ but minimize ω. Here, ω_{*E} is the energetic-particle diamagnetic drift frequency. Thus, for shear Alfvén waves, one needs to minimize $|\omega| \propto |nq - m|$ subject to $n \gg 1$. This is achieved by first localizing $\delta\phi(r, m)$ around the mode-rational surface at $r - r_m$ where $nq(r_m) = m$; and then limit the mode localization width to $\Delta r_m \sim O(\Delta r_s)$ with $\Delta r_s = 1/nq'$ being the distance between the neighboring mode-rational surfaces. With $n \gg 1$, we have $|\Delta r_s|/|r_m| \sim 0(1/nq) \ll 1$ and, therefore, there are two disparate radial scale lengths; the fast local scale Δr_s and the slow global scale a. We can then proceed with the analysis by adopting the standard ballooning formalism [20–22].

Ignoring global variation due to equilibrium profile for now, we may assume translational invariances among $\delta\phi(r, m)$; i.e.,

$$\delta\phi(r, m) = \delta\phi(nq - m) = \delta\phi(\tau - m).$$

Here, $\tau = nq$ is a dimensionless radial "flux" coordinate. Letting $\delta\Phi(\theta)$ be the Fourier conjugate of $\delta\phi(\tau - m)$; i.e., $\delta\phi(\tau - m) = \int_{-\infty}^{\infty} d\theta\, \delta\Phi(\theta) \exp[-i(\tau - m)\theta]$ and adopting ideal MHD description as well as the well-known (s, α) model equilibrium [23], the corresponding shear Alfvén wave equation becomes [6]

$$\left\{ \frac{d}{d\theta} f \frac{d}{d\theta} + \Omega^2(1 + 2\varepsilon_0 \cos\theta) f + \alpha[\cos\theta + (s\theta - \alpha \sin\theta)\sin\theta] \right\} \delta\Phi = 0; \tag{21}$$

where $f = 1 + (s\theta - \alpha \sin\theta)^2$, $\Omega^2 = (\omega/\omega_A)^2$, $\varepsilon_0 = 2(r_{m0}/R + \Delta')$ and Δ is the Shafranov shift. Note, in Eq. (21), first, second and third terms correspond, respectively to the effects of field-line bending, finite inertial, and finite-curvature coupling to the convective component of the perturbed pressure. The third term gives rise to the well-known ballooning/interchange drive. Letting $\delta\psi = f^{1/2}\delta\Phi$, Eq. (21) can be written in the standard Schrödinger form

$$\left[\frac{d^2}{d\theta^2} + V_I(\theta) \right] \delta\psi = 0; \tag{22}$$

where

$$V_I(\theta) = \Omega^2(1 + 2\varepsilon_0 \cos\theta) + \frac{\alpha \cos\theta}{f} - \frac{(s - \alpha \cos\theta)^2}{f^2}. \tag{23}$$

Let us first consider the toroidal SAW continuous spectrum; that is, values of Ω^2 such that $\delta\phi(\tau - m)$ becomes singular. This can be equivalently analyzed in the $|\theta| \to \infty$ limit of Eq. (22); i.e.,

$$\left[\frac{d^2}{d\theta^2} + V_{IE}(\theta) \right] \delta\psi_E = 0; \tag{24}$$

where

$$V_{IE}(\theta) = \Omega^2(1 + 2\varepsilon_0 \cos\theta). \tag{25}$$

Equation (24) is the standard Mathieu's equation. Hence, $\delta\psi_E$ is stable (purely oscillatory) for Ω^2 belongs to Ω_T^2, which consists of $[0, \infty]$ except narrow frequency gaps, $(\Delta\Omega)_j \sim O(\varepsilon_0^j)$, centered about the characteristic frequencies at $\Omega_j^2 = (j/2)^2$ for $j = 1, 2, \ldots$. Since purely oscillatory $\delta\psi_E$ results in singular $\delta\phi(\tau - m)$, Ω_T^2 is the toroidal SAW continuum. Ω_T^2 can be alternatively understood in the $(\tau - m)$ radial coordinate. Note that, in the cylindrical limit, the SAW continuum for the individual poloidal harmonics $\delta\phi(nq - m) = \delta\phi(\tau - m)$ is $\Omega_c^2 = (\tau - m)^2$; i.e., $[0, \infty]$. The finite toroidicity, however, introduces coupling between the mth and $(m + j)$th poloidal harmonics and break the continuum at $\tau - m = \tau_j$ where Ω_{cm} and $\Omega_{c(m+j)}$ become degenerate. Thus, $\tau_j = j/2$ and, correspondingly, $\Omega_j^2 = (j/2)^2$.

Noting that, for Ω^2 inside the frequency gaps, $\delta\psi_E$ can decay exponentially in $|\theta|$, one important discovery [14] is that, for appropriate parameters, a potential well can be formed around $|\theta| \sim 0(1)$; leading to *discrete* marginally stable eigenmodes. Since, in the current model, the $j = 1$ toroidal Alfvén gap (TAG) has the lowest frequency and the widest gap

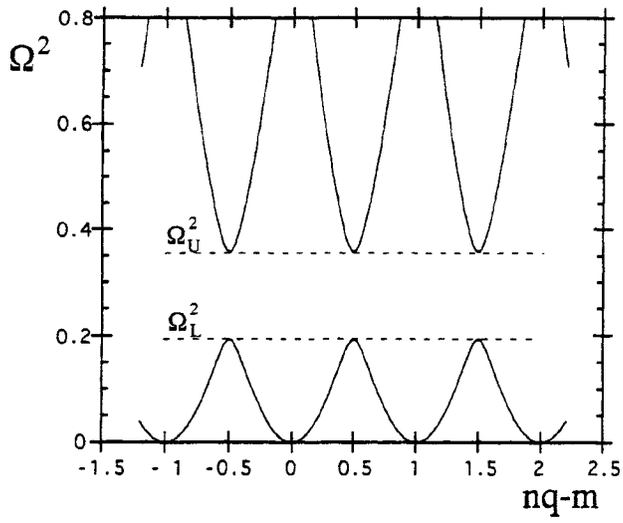


Fig. 1. Sketch of the toroidal shear Alfvén continuous spectrum $\Omega^2 = (\omega/\omega_A)^2$ versus $nq - m$.

$[\Delta\Omega \sim 0(\varepsilon_0)]$, it will be our focus from now on. Specifically, TAG corresponds to $\Omega_L^2 \leq \Omega^2 \leq \Omega_U^2$; where

$$\Omega_{U,L}^2 = [4(1 \mp \varepsilon_0)]^{-1}. \tag{26}$$

Figure 1 is a sketch of the corresponding SAW continuum versus $nq - m = \tau - m$. The discrete eigenmode lies inside TAG is then the well-known toroidal shear Alfvén eigenmode or TAE for short.

Employing the smallness parameter $\varepsilon_0 \ll 1$, the (radially) local TAE dispersion relation can be derived via an asymptotic matching analysis. Specifically, we denote $\theta_0 \sim 0(1)$ and $\theta_1 \sim 0(1/\varepsilon_0) \gg 1$ as the two scales. In the external region, $|\theta| \sim \theta_1$, we have Eq. (24). Substituting $\delta\psi_E$ as

$$\delta\psi_E = A(\theta_1)\cos(\theta_0/2) + B(\theta_1)\sin(\theta_0/2) \tag{27}$$

into Eq. (24), A and B can be readily solved to yield

$$\delta\psi_E = \left[(-\Gamma_-)^{1/2}\cos\frac{\theta_0}{2} + \Gamma_+^{1/2}\sin\frac{\theta_0}{2}\right]\exp(-\hat{\gamma}\theta_1); \quad \text{for } \theta > 0 \tag{28}$$

where

$$\Gamma_{+,-} = \Omega^2 - \Omega_{L,U}^2, \tag{29}$$

$\hat{\gamma} = (-\Gamma_-\Gamma_+)^{1/2}$, and only even solution is kept here. In the internal region $\theta = \theta_0 \sim 0(1)$, Eq. (22) and (23) become

$$\left[\frac{d}{d\theta_0^2} + V_{II}(\theta_0)\right]\delta\psi_I = 0; \tag{30}$$

where

$$V_{II}(\theta_0) = 1/4 + \alpha\cos\theta_0/f - (s - \alpha\cos\theta_0)^2/f^2. \tag{31}$$

Assuming $s, \alpha < 1$, we may assume $\delta\psi_I \simeq (-\Gamma_-)^{1/2}\cos\theta_0/2$ and use Eq. (30) to evaluate the asymptotic coefficient of the $\sin\theta_0/2$ term. Matching it with that given by Eq. (28); i.e., $\Gamma_+^{1/2}$, then yield the desired TAE dispersion relation [6]

$$(-\Gamma_+/\Gamma_-)^{1/2} = \delta T_f = \pi s(1 - \alpha/s^2)/4. \tag{32}$$

Equation (31) dictates that TAE exists only if $\delta T_f > 0$ or $\alpha < \alpha_c \simeq s^2$ in the present equilibrium model. For $\alpha \geq \alpha_c$, TAE merges into the lower SAW continuum.

As discussed in Section 2, introducing kinetic Alfvén waves (KAW) removes singularity associated with SAW continuum. It, therefore, may be expected that KAW can resolve the toroidal SAW continuum into discrete eigenmodes. Specifically, we note that the potential for the corresponding Schrödinger equation, Eq. (22), becomes

$$V_2(\theta) = V_1(\theta) - s^4\rho_K^2\theta^4/f; \tag{33}$$

where

$$\rho_K^2 = \hat{\rho}_K^2 - ik_\theta^2 c^2\eta/16\pi\omega, \tag{34}$$

$V_1(\theta)$ given by Eq. (23), ρ_K^2 given by Eq. (18) and η corresponds to the finite-resistivity effect [14]. Assuming $|\varepsilon_0/2|^3 > |s\rho_K|^2$ such that the eigenmodes are highly extended along θ, we let $|\theta| \gg 1$ and $V_2(\theta)$ then reduces to

$$V_{2E}(\theta) = \Omega^2(1 + 2\varepsilon_0\cos\theta_0) - s^2\rho_K^2\theta_1^2; \tag{35}$$

where we have explicitly denoted the θ_0 *and* θ_1 scales. Substituting $\delta\psi_E$ as given by Eq. (27) into Eq. (24), we have

$$dA/d\theta_1 = (\Gamma_- - s^2\rho_K^2\theta_1^2)B, \tag{36}$$

$$dB/d\theta_1 = -(\Gamma_+ - s^2\rho_K^2\theta_1^2)A. \tag{37}$$

In the case of upper toroidal SAW continuum, $\Omega^2 \simeq \Omega_U^2$, $\Gamma_+ \simeq \varepsilon_0/2$, and Eqs (36) and (37) can be combined to become

$$\left[\frac{d^2}{d\theta_1} + \frac{\varepsilon_0}{2}(\Gamma_- - s^2\rho_K^2\theta_1^2)\right]B(\theta_1) = 0. \tag{38}$$

Consequently, the upper continuum is discretized into the upper kinetic TAE (KTAE) given by the following dispersion relation, for $n = 0, 1, \ldots,$

$$\Omega^2 - \Omega_U^2 \simeq (2n + 1)s\rho_K(2/\varepsilon_0)^{1/2}. \tag{39}$$

Similarly, one can derive the following dispersion relation for the lower KTAE;

$$\Omega^2 - \Omega_L^2 \simeq -i(2n + 1)s\rho_K(2/\varepsilon_0)^{1/2}. \tag{40}$$

Recalling discussions in Section 2 that in the limit of no (collisionless and collisional) dissipations, KAW is propagating when $\omega^2 > \omega_{An}^2(x)$; upper KTAE thus corresponds to KAW trapped in the potential well formed by the upper toroidal SAW continuum (cf. Fig. 1). The lower toroidal SAW continuum, meanwhile, gives rise to a potential hill and, hence, the lower KTAE experiences convective damping as clearly indicated by Eq. (40).

4. Kinetic excitation of toroidal Alfvén modes

In magnetically confined fusion plasmas a wide variety of energetic ions may exist, e.g. those produced by neutral beam/ICRH heating and/or α-particles from D–T fusion reactions. The characteristic dynamic frequencies of these energetic ions are the transit frequency, ω_{tE}, for particles moving freely along magnetic field lines; and the bounce frequency, ω_{bE}, and the precession rate, $\bar{\omega}_{dE}$, for particles trapped between magnetic mirror points and moving along banana orbits at a rate ω_{bE}. Since the toroidal Alfvén frequency gap is located at $\omega_{TAG} \approx \omega_{tE}, \omega_{bE}, \bar{\omega}_{dE}$, collective SAW instabilities categorized as toroidal Alfvén modes (TAM) may tap expansion free energy from energetic particles and be resonantly excited.

The generalization of the SAW equation, Eq. (22), to include resonant TAM excitations by energetic particles is [16, 19]:

$$\left[\frac{d^2}{d\theta^2} + V_2(\theta)\right]\delta\psi - \sum_j \frac{q^2R^2}{k_\chi^2}\frac{\eta_j}{f^{1/2}}\langle\omega_d J_0(\lambda_\rho)\delta G\rangle_j = 0; \tag{41}$$

where $V_2(\theta)$ is given by Eq. (33) and the last term in Eq. (41) accounts for the resonant interaction of the mode with the particles magnetic drifts. Hence, it includes the energetic particles drive and electron and ion "drift"-Landau damping. Note that J_0 is the Bessel function of the first kind and zero index, with argument $\lambda_{\rho_j} = k_\perp (m_j c/e_j B) v_\perp$, $k_\perp^2 = k_\chi^2 + k_r^2 = k_\chi^2 f$, $\eta_j = 4\pi\omega e_j/c^2$, $\omega_{dj}(\theta) = \Omega_{dj} g(\theta)$, $g(\theta) = \cos\theta + [s\theta - \alpha\sin\theta]\sin\theta$, $\Omega_{dj} = k_\chi c m_j (v_\perp^2/2 + v_\parallel^2)/e_j BR$ and $\langle\cdots\rangle = \int d^3v(\cdots)$. The distribution function δG_j is derived from the gyrokinetic equation [6]

$$[\omega_t \partial_\theta - i(\omega - \omega_d)]_j \delta G_j = i\left(\frac{e}{m}\right)_j Q F_{0j} \times \frac{1}{f^{1/2}}\left(\frac{\omega_d}{\omega}\right)_j J_0(\lambda_{\rho_j})\delta\psi, \tag{42}$$

where $\omega_t = v_\parallel/qR$ is the transit frequency, $QF_{0j} = (\omega\partial_E + \hat{\omega}_*)_j F_{0j}$, $E = v^2/2$, and $\hat{\omega}_{*j} F_{0j} = (m_j c/e_j B)(\boldsymbol{k}\times \boldsymbol{e}_\parallel)\cdot\nabla F_{0j}$. Equations (41) and (42) define the coupled one-dimensional (along a given magnetic flux tube) integro-differential eigenvalue problem for toroidal Alfvén modes. These equations are generally difficult to solve. However, following the analysis of Section 3, Eqs (41) and (42) may be solved for a large aspect-ratio tokamak equilibrium, by asymptotically matching the solutions of two regions: the external long-scale $|\theta| \sim \theta_1 \sim O(1/\epsilon_0)$ [i.e., $\Delta r \sim O(\epsilon_0/nq')$ "gap"] region, where toroidal coupling is important; and the internal short scale $|\theta| \sim \theta_0 \sim O(1)$ [i.e., $\Delta r \sim O(1/nq')$ "ideal"] region.

With the formal $|k_\chi \rho_E| \sim \epsilon_0^{1/2}$ ordering [16, 24], the energetic particles dynamics may be neglected in the gap region, since $|k_\perp \rho_E| \sim \epsilon_0^{-1}|k_\chi \rho_E| \sim \epsilon_0^{-1/2} \gg 1$ and energetic ions cannot excite waves with perpendicular wavelengths smaller than their typical orbit sizes. This fact demonstrates the importance of accounting for finite orbit widths of fast particles. On the contrary, core plasma ions and electrons contributions must be maintained in the $|\theta| \sim \theta_1$ region, since their orbit sizes, $|k_\perp \rho_{iC}| \sim (T_C/T_E)^{1/2}|k_\perp\rho_E| \sim \epsilon_0^{1/2}$, may be ignored.

In Section 3, it has been shown that the solution of Eq. (41) in the external ($|\theta| \sim \theta_1$) region has the form

$$\delta\psi_E = \epsilon_P^{(\pm)}[A(\theta_1)\cos(\theta_0/2) + B(\theta_1)\sin(|\theta_0|/2)], \tag{43}$$

where ($\pm$) refers to the sign of θ_1, and $\epsilon_P^{(\pm)}$ give the parity of the mode structure in θ_1. Taking $\epsilon_P^{(+)} \equiv 1$ for reference, $\epsilon_P^{(-)} = \pm 1$ corresponds to even/odd mode structures, respectively. The functions $A(\theta_1)$ and $B(\theta_1)$ satisfy the following equations:

$$A'(\theta_1) = (\hat{\Gamma}_- - s^2\rho_K^2\theta_1^2)B(\theta_1) + i\beta_2 A(\theta_1),$$
$$B'(\theta_1) = -(\hat{\Gamma}_+ - s^2\rho_K^2\theta_1^2)A(\theta_1) + i\beta_2 B(\theta_1), \tag{44}$$

where [6]

$$\hat{\Gamma}_{+,-} = \Omega^2 - \Omega_{L,U}^2 - \beta_1, \tag{45}$$

$$\beta_1 = \frac{\pi q^2}{B^2}\sum_{j=e,i} m_j\left(\frac{v_\perp^2}{2} + v_\parallel^2\right)^2 QF_{0j} \times \left(\frac{\omega}{\omega_t^2/4 - \omega^2} + \frac{\omega}{9\omega_t^2/4 - \omega^2}\right)_j, \tag{46}$$

$$\beta_2 = \frac{\pi q^2}{B^2}\sum_{j=e,i} m_j\left(\frac{v_\perp^2}{2} + v_\parallel^2\right)^2 QF_{0j} \times \left(\frac{\omega_t/2}{\omega_t^2/4 - \omega^2} - \frac{3\omega_t/2}{9\omega_t^2/4 - \omega^2}\right)_j. \tag{47}$$

Here, β_1 and β_2 terms account for mode resonances with the core plasma particles.

In the internal $|\theta| \sim \theta_0 \sim O(1)$ ideal region, meanwhile, Eq. (41) reduces to

$$\left[\frac{d^2}{d\theta^2} + \frac{1}{4} + \frac{\alpha\cos\theta_0}{f} - \frac{(s - \alpha\cos\theta_0)^2}{f^2}\right]\delta\psi_I - \sum_j \frac{q^2R^2}{k_\chi^2}\frac{\eta_j}{f^{1/2}}\langle\omega_d J_0(\lambda_\rho)\delta G\rangle_j = 0. \tag{48}$$

From Eq. (48), we may construct the following quadratic form [16, 24]

$$\delta\psi_I^* \frac{d\delta\psi_I}{d\theta}\bigg|_{-\infty}^{+\infty} - 2\delta W_f - 2\delta W_K = 0, \tag{49}$$

where δW_f is the ideal MHD contribution to the potential energy perturbation

$$\delta W_f = \frac{1}{2}\int_{-\infty}^{\infty} d\theta \left[\left|\frac{d\delta\psi_I}{d\theta}\right|^2 + \left(\frac{(s - \alpha\cos\theta_0)^2}{f^2} - \frac{\alpha\cos\theta_0}{f}\right)|\delta\psi_I|^2\right], \tag{50}$$

and δW_K is the analogous contribution due to energetic particles compression

$$\delta W_K = \frac{1}{2}\frac{q^2R_0^2}{k_\chi^2}\eta_E\int_{-\infty}^{\infty} d\theta\langle\delta S^*\delta G\rangle_E, \tag{51}$$

with

$$\delta S_E = \omega_{dE} f^{-1/2} J_0(\lambda_{\rho E})\delta\psi_I. \tag{52}$$

The asymptotic matching condition between $\delta\psi_E$ and $\delta\psi_I$ reads

$$\delta\psi_I^* \frac{d\delta\psi_I}{d\theta}\bigg|_{-\infty}^{+\infty} = A(0)^* B(0), \tag{53}$$

$A(0)$ and $B(0)$ being the values at $\theta_1 = 0$ of the functions satisfying Eq. (44). Thus, Eq. (49) leads to the following TAM local dispersion relation

$$\frac{B(0)}{A(0)} = \delta T_f + \delta T_K. \tag{54}$$

Here, for simplicity of notation, we have introduced the quantities $\delta T_f = 2\delta W_f/|A(0)|^2$ and $\delta T_K = 2\delta W_K/|A(0)|^2$.

From Section 3, we know that the $s, \alpha < 1$ case is particularly simple to handle analytically. Thus, we will use the same assumption also in the discussion on TAM local stability, starting from the local dispersion relation Eq. (54). For $s, \alpha < 1$, a good trial function to be used in Eq. (50) is (cf. Section 3) $\delta\psi_I = A(0)\cos(\theta/2)$, which yields $\delta T_f = (s\pi/4)(1 - \alpha/\alpha_c)$, given by Eq. (32). As to the contribution of energetic ions compression to the potential energy variation, it may be computed for passing and trapped particles respectively. The calculation involves the determination of the particles perturbed distribution functions, δG_E, from Eq. (42), and then of δS_E as defined in Eq. (52). All these details are thoroughly discussed in Refs [16, 19, 24]; thus, we will only quote, here, the final results. That is, $\delta T_K = \delta T_{K,u} + \delta T_{K,T}$, where $\delta T_{K,u}$ and $\delta T_{K,T}$ are, respectively, the passing and trapped particle contributions:

$$\delta T_{K,u} = \frac{\pi^2}{4s}\frac{e^2}{mc^2}\frac{q^2R_0^2}{k_\chi^2}\left\langle\frac{\Omega_d^2 QF_0}{\Delta(1+\Delta^2)^{3/2}} \times \left[\frac{\omega}{\omega_t^2/4 - \omega^2} + \frac{\omega}{9\omega_t^2/4 - \omega^2}\right]\right\rangle, \tag{55}$$

$$\delta T_{K,T} = \frac{4\pi^2 e^2}{mc^2} q R_0 B_0 \sum_{\sigma=\pm} \int dE \int d\mu \left(\frac{\Omega_d}{k_\chi}\right)^2 \tau_b Q F_0 \times \left[\frac{1}{\bar{\omega}_d - \omega} + \frac{\theta_b^2/8s}{\Delta_T(1+\Delta_T^2)^{3/2}} \frac{\omega - \bar{\omega}_d}{\omega_b^2 - (\omega - \bar{\omega}_d)^2}\right]. \quad (56)$$

Here, $\Delta^2 = (k_\chi^2/4)(\rho_L^2 + \rho_d^2/2)$, $\rho_d^2 = \Omega_d^2/(k_\chi^2\omega_t^2)$, $\Delta_T^2 = (k_\chi^2/4)(\rho_L^2 + \theta_b^2\rho_b^2/2)$, θ_b is the bounce angle for trapped particles, and $\rho_b^2 = \Omega_d^2/(k_\chi^2\omega_b^2)$. Furthermore, a summation on all energetic particles species is implicitly assumed. Equation (55) accounts for the well known $v_\parallel = v_A$ and $v_\parallel = v_A/3$ resonances of TAM with circulating particles, whereas Eq. (56) describes the resonant interaction of TAM with the precession rate of trapped energetic ions and the first bounce resonance. Higher order resonances of TAM with the bounce motion of trapped particles occur at higher frequencies and they are usually negligible [24].

Equations (55) and (56) assume the formal ordering $k_r\rho_E \sim \epsilon_0^{-1/2}$, i.e., large particle orbits. They predict energetic particles responses independent on the mode number for $1 < k_r\rho_E < \epsilon_0^{-1}$, and a $(k_\chi\rho_E)^{-3}$ scaling for $k_r\rho_E > \epsilon_0^{-1}$ [16,19,24]. The small orbit case, $k_r\rho_E < 1$, can be handled in the present theoretical approach by assuming $\delta T_{K,u} = \delta T_{K,T} = 0$ and by extending Eqs (46) and (47) to include the energetic particle contribution, which will scale as $\sim k_\chi\rho_E$ [6].

With the help of Eqs (37), (55) and (56), the local dispersion relation, Eq. (54), becomes [16,19]

$$\frac{B(0)}{A(0)} = \frac{s\pi}{4}\left(1 - \frac{\alpha}{\alpha_c}\right) + \delta T_{K,u} + \delta T_{K,T}. \quad (57)$$

Following the analysis presented in Section 3, we will discuss the linear stability of TAM in the ideal limit first (i.e., no core plasma kinetic effects), and then the new features of the TAM spectrum due to $\sim s^2\rho_K^2$ terms in Eq. (44) will be analyzed.

4.1. *Ideal TAM spectrum*

In the ideal limit, $s^2\rho_K^2 \to 0$, $\delta\psi_E$ is the same as that given by Eq. (28); with $\Gamma_\pm$ and $\hat{\gamma}$ replaced, correspondingly, by $\hat{\Gamma}_\pm$ and $\hat{\gamma} = (-\hat{\Gamma}_-\hat{\Gamma}_+)^{1/2}$. As a consequence, the local dispersion relation, Eq. (57), becomes

$$\left(-\frac{\hat{\Gamma}_+}{\hat{\Gamma}_-}\right)^{1/2} = \frac{s\pi}{4}\left(1 - \frac{\alpha}{\alpha_c}\right) + \delta T_{K,u} + \delta T_{K,T}, \quad (58)$$

with the causality constraint [16]

$$\Re(-\hat{\Gamma}_+/\hat{\Gamma}_-)^{1/2} > 0. \quad (59)$$

For sufficiently small energetic particle response, Eq. (58) satisfies the causality constraint provided $\alpha < \alpha_c$. Then, Eq. (58) becomes the well-known TAE local dispersion relation in the small shear limit, with the additional contribution of energetic particles with finite orbit-widths. The corresponding mode structure along magnetic field lines is even, since $B(0) \simeq 0$ and, as a consequence, $\epsilon_P^{(-)} = 1$ in Eq. (43). From Eq. (58), the real mode frequency and growth rate of TAE modes for $s \ll 1$ and $\alpha < \alpha_c$ are expressed as follows

$$\Omega_r^2 = \Omega_L^2 + \Re\beta_1 + \frac{\epsilon_0}{2} \times \left[\Re(\delta T_{K,u} + \delta T_{K,T}) + \frac{s\pi}{4}\left(1 - \frac{\alpha}{\alpha_c}\right)\right]^2, \quad (60)$$

$$\frac{\gamma}{\omega_r} = 2\Im\beta_1 + 2\epsilon_0\Im(\delta T_{K,u} + \delta T_{K,T}) \times \left[\Re(\delta T_{K,u} + \delta T_{K,T}) + \frac{s\pi}{4}\left(1 - \frac{\alpha}{\alpha_c}\right)\right]. \quad (61)$$

For $\alpha > \alpha_c$, it has been shown that TAE's merge into the lower Alfvén continuum and become strongly damped [18]. In the SAW continuum, $(-\hat{\Gamma}_+/\hat{\Gamma}_-)^{1/2}$ in Eq. (58) is analytically continued as $i(\hat{\Gamma}_+/\hat{\Gamma}_-)^{1/2}$, and collective plasma oscillations may be excited only if the energetic particles drive exceeds the stabilizing effect of *continuum damping* $\sim i(\hat{\Gamma}_+/\hat{\Gamma}_-)^{1/2}$. Meanwhile, a substantial contribution from energetic particles compression is also required in order to satisfy the causality constraint, Eq. (59). Thus, resonant excitation of collective modes in the SAW continuum crucially depends on the presence of energetic particles in excess of a certain threshold, determined by the background of continuous plasma oscillations. This demonstrates why the dynamics of energetic particles cannot be treated as a perturbation to that of the core plasma in the description these modes, called energetic particles continuum modes (EPM) [16]. Close to marginal stability, EPM real frequency and growth rate are readily obtained from Eq. (58)

$$\Re(\delta T_{K,u}(\omega_r) + \delta T_{K,T}(\omega_r)) + \frac{s\pi}{4}\left(1 - \frac{\alpha}{\alpha_c}\right) = 0, \quad (62)$$

$$\frac{\gamma}{\omega_r} = -\frac{\Im(\delta T_{K,u} + \delta T_{K,T}) - \left(\sqrt{\hat{\Gamma}_+/\hat{\Gamma}_-}\right)_{\omega_r}}{\omega_r \partial\Re(\delta T_{K,u} + \delta T_{K,T})/\partial\omega_r}. \quad (63)$$

The corresponding EPM mode structure along magnetic field lines is even, as in the case of TAE, and its frequency is located within the lower Alfvén continuum.

In the $s, \alpha < 1$ limit, it may be shown that Eq. (58) is not the only existent TAM branch. In fact, it may be demonstrated that an odd parity TAM mode exists, which satisfies [19]

$$\frac{A(0)}{B(0)} = \left(-\frac{\hat{\Gamma}_-}{\hat{\Gamma}_+}\right)^{1/2} = -\left[\frac{s\pi}{4}\left(1 + \frac{\alpha}{\alpha_c}\right) + \delta T_{K,u}\right]. \quad (64)$$

The parity of the mode structure along the magnetic field line is odd, in the present case, since $A(0) \simeq 0$, i.e., $\epsilon_P^{(-)} = -1$ in Eq. (43). One important feature of Eq. (64) is that the causality constrain, Eq. (59), is never satisfied for perturbative energetic particles response. This is consistent with the fact that, in the $s, \alpha < 1$ limit, no TAM modes exist within the Alfvén frequency gap other than the even TAE, described by Eqs (60) and (61). Equation (64), thus, predicts only the resonant excitation of an odd EPM in the upper Alfvén continuum when the energetic particles drive exceeds the *continuum damping* $(-\hat{\Gamma}_-/\hat{\Gamma}_+)^{1/2} \to -i(\hat{\Gamma}_-/\hat{\Gamma}_+)^{1/2}$. Close to marginal stability, the odd EPM must satisfy

$$\Re\delta T_{K,u}(\omega_r) + \frac{s\pi}{4}\left(1 + \frac{\alpha}{\alpha_c}\right) = 0, \quad (65)$$

$$\frac{\gamma}{\omega_r} = -\frac{\Im\delta T_{K,u} - \left(\sqrt{\hat{\Gamma}_-/\hat{\Gamma}_+}\right)_{\omega_r}}{\omega_r \partial\Re\delta T_{K,u}/\partial\omega_r}. \quad (66)$$

There is a crucial difference between the EPM and the usual TAE branch, which is evident by comparing Eq. (61) with Eqs (63) and (66). TAE's are nearly threshold-less instabilities, whereas EPM's have instability thresholds to overcome, due to the finite continuum damping. The threshold condition is [16]

$$\alpha_E > \alpha_{Ec} \simeq O(v(\omega_r)), \quad (67)$$

where $v(\omega_r) = \sqrt{\hat{\Gamma}_+/\hat{\Gamma}_-}|_{\omega_r}$ for the even branch, and $v(\omega_r) = \sqrt{\hat{\Gamma}_-/\hat{\Gamma}_+}|_{\omega_r}$ for the odd branch.

4.2. *Kinetic TAM spectrum*

In this Section we will comment on the new features of the TAM spectrum, excited by energetic alpha particles, which appear when core plasma kinetic effects $\sim s^2\rho_K^2$ are fully retained in Eq. (44). Following Section 3, we will make the reasonable assumption $|s^2\rho_K^2| < |\epsilon_0\Omega^2|^3$. From Eq. (44), it is then readily seen that core plasma kinetic effects weakly modify the dynamics of ideal TAE, for which $\hat{\Gamma}_+ \sim \hat{\Gamma}_- \sim \epsilon_0$ and $A(\theta_1)$, $B(\theta_1)$ vary on the scale $\theta_1 \sim O(1/\epsilon_0)$. In fact, it is possible to demonstrate that the TAE suffers only from an exponentially small radiative damping [15], due to a subdominant energy tunnelling to very small wavelengths, where kinetic dissipation takes place. Core plasma kinetic effects become crucial for the mode dynamics when $\hat{\Gamma}_+$ or $\hat{\Gamma}_- \to 0$, i.e., when the accumulation points of the SAW continuum are approached.

Consider, first, the case of the lower continuum accumulation point; i.e., $|\hat{\Gamma}_+| \ll \epsilon_0$ and $\hat{\Gamma}_- \simeq -2\epsilon_0\Omega^2$. In this limit, Eq. (44) gives $B(\theta_1) = -A'(\theta_1)/2\epsilon_0\Omega^2$ and $A = U(a, x)$, $U(a, x)$ being the Whittaker's parabolic cylinder function and

$$x = \exp(i\pi/4)(8\epsilon_0\Omega^2 s^2\rho_K^2)^{1/4}\theta_1,$$

$$a = \frac{-i\hat{\Gamma}_+}{\sqrt{2}s\rho_K/\sqrt{\epsilon_0\Omega^2}}. \tag{68}$$

We find, thus,

$$\frac{A(0)}{B(0)} = \frac{\exp(-i\pi/4)}{(2\Delta_K)^{1/4}}\frac{\Gamma(1/4+a/2)}{\Gamma(3/4+a/2)}, \tag{69}$$

with $\Delta_K = s^2\rho_K^2/(\epsilon_0\Omega^2)^3$. Equation (69), substituted into Eqs (57) and (64), gives, respectively, even and odd KTAE modes in the lower continuum. To the lowest order, it is readily seen that even KTAE modes ($B(0) \simeq 0$) satisfy $a \simeq -(2N + 1/2)$, with N being the mode quantum number and a non-negative integer. Meanwhile, $a \simeq -(2N + 3/2)$ for odd modes ($A(0) \simeq 0$). Considering also next order corrections, the even KTAE dispersion relation is

$$\frac{\hat{\Gamma}_+}{\epsilon_0\Omega^2} \simeq -i\sqrt{2\Delta_K}\left\{\frac{1}{2} + 2N - \frac{(2N+1)!!}{(2N+1)} \times \exp(-i\pi/4)\frac{[\delta T_{K,u}+\delta T_{K,T}+\frac{1}{4}s\pi(1-\alpha/\alpha_c)]}{(2\Delta_K)^{1/4}2^{N-1}N!\sqrt{\pi}}\right\}, \tag{70}$$

whereas the odd KTAE branch turns out to be

$$\frac{\hat{\Gamma}_+}{\epsilon_0\Omega^2} \simeq -i\sqrt{2\Delta_K}\left\{\frac{3}{2} + 2N - \frac{(2N+1)!!}{2^N N!} \times \exp(i\pi/4)\frac{(2\Delta_K)^{1/4}}{\sqrt{\pi}}\left[\delta T_{K,u} + \frac{s\pi}{4}\left(1+\frac{\alpha}{\alpha_c}\right)\right]\right\}. \tag{71}$$

Note that, for $|\Delta_K| < 1$, even mode structures in the lower continuum tend to be more influenced by energetic particles than odd modes. Note also that Eqs (70) and (71) reduce, in the lowest order, to Eq. (40), as expected.

Consider, now, the case of KTAE modes excited near the upper continuum accumulation point; i.e., $|\hat{\Gamma}_-| \ll \epsilon_0$ and $\hat{\Gamma}_+ \simeq 2\epsilon_0\Omega^2$. Equation (44), then, gives $A(\theta_1) = -B'(\theta_1)2\epsilon_0\Omega^2$ and $B = U(a, x)$, with

$$x = (8\epsilon_0\Omega^2 s^2\rho_K^2)^{1/4}\theta_1,$$

$$a = -\frac{\hat{\Gamma}_-}{\sqrt{2}s\rho_K/\sqrt{\epsilon_0\Omega^2}}. \tag{72}$$

We find, thus,

$$\frac{A(0)}{B(0)} \simeq (2\Delta_K)^{1/4}\frac{\Gamma(3/4+a/2)}{\Gamma(1/4+a/2)}. \tag{73}$$

Proceeding as in the lower continuum case, the even KTAE dispersion relation in the upper SAW continuum is

$$\frac{\hat{\Gamma}_-}{\epsilon_0\Omega^2} \simeq \sqrt{2\Delta_K}\left\{\frac{3}{2} + 2N + \frac{(2N+1)!!}{2^N N!} \times \frac{(2\Delta_K)^{1/4}}{\sqrt{\pi}}\left[\delta T_{K,u} + \delta T_{K,T} + \frac{s\pi}{4}\left(1-\frac{\alpha}{\alpha_c}\right)\right]\right\}. \tag{74}$$

Similarly, the odd KTAE branch is found to be

$$\frac{\hat{\Gamma}_-}{\epsilon_0\Omega^2} \simeq \sqrt{2\Delta_K}\left\{\frac{1}{2} + 2N + \frac{(2N+1)!!}{(2N+1)} \times \frac{[\delta T_{K,u} + \frac{1}{4}s\pi(1+\alpha/\alpha_c)]}{(2\Delta_K)^{1/4}2^{N-1}N!\sqrt{\pi}}\right\}. \tag{75}$$

Note that the roles of even and odd mode structures are inverted with respect to the lower continuum case and that, now, the odd branch is most influenced by energetic particles. Similarly, Eqs (74) and (75) reduce, in the lowest order, to Eq. (39).

As already noticed in Section 3, the lower KTAE is strongly damped due to wave energy convection away from the mode localization region. The upper KTAE, instead, suffers of a much weaker damping, essentially due to collisions with trapped electrons [25], which determine $\Im\Delta_K$. In both cases, energetic particles give an effect on the mode dynamics which results in a frequency shift and/or drive at most comparable with the typical frequency separation in the KTAE spectrum. This is the consistency requirement of perturbation theory leading to Eqs (70)–(71) and (74)–(75). Therefore, the lower KTAE is never destabilized by energetic particles, whereas the upper KTAE may be only weakly unstable.

If KTAE are driven strongly enough that the perturbative treatment of energetic particle dynamics fails, the even and odd ideal EPM branches get excited and emerge, respectively, from the closest even lower KTAE and odd upper KTAE [19]. This may be seen from Eqs (70) and (75), for which energetic particles contribution is strongest. Using the Stirling approximation to factorials, the condition for break down of perturbative analyses reads, respectively,

$$|\delta T_K| \gtrsim N^{1/2}|\Delta_K|^{1/4} \sim \left|\frac{\hat{\Gamma}_\pm}{\epsilon_0\Omega^2}\right|^{1/2}, \tag{76}$$

which is equivalent to the threshold condition for EPM excitation, Eq. (67).

This result demonstrates that the most unstable energetic particles driven TAM are ideal modes. In the absence of TAE ($\alpha > \alpha_c$) or EPM [Eq. (67) not satisfied], only moderately unstable upper KTAE can be excited.

5. Global mode structures of TAM

In the previous Sections, a detailed discussion of SAW instabilities excited by energetic particles was presented from the point of view of local stability analyses of these modes on a given magnetic flux surface. All results, thus, have been expressed in terms of local parameters characterizing the plasma equilibrium and the energetic particles distribution function.

However, it has been shown that TAM may actually have rather extended radial mode structures [17–19], which makes it crucial to account for radial equilibrium profiles of both

core plasma and energetic particle component. Therefore, two-dimensional (2-D) global analyses are necessary to properly assess the stability properties of Alfvén waves in tokamak plasmas.

It has been pointed out in Section 4 that TAM may be excited by tapping the expansion free energy of energetic particles. Thus, TAM may be characterized as drift-wave-like instabilities, for which the growth rate $\gamma \propto \omega_{*E}$. Thus, most unstable modes tend to have toroidal mode number $n \gg 1$. We will shortly see that $1/n$ is the expansion parameter that makes it possible to use a multiple scale WKB formalism to perform 2-D eigenmode stability analyses, with the great advantage of reducing a fully 2-D eigenvalue problem to two nested 1-D ones.

As noted in Section 3, the perturbed scalar potential may be Fourier decomposed as

$$\delta\phi(r, \chi, \xi, t) = \exp(-i\omega t + in\xi) \sum_m \delta\phi(r, m) \exp(-im\chi). \quad (20)$$

Furthermore, as also pointed out in Section 3, for $n \gg 1$ the poloidal harmonics $\delta\phi(r, m)$ are characterized by two distinct spatial scales: the local scale $\Delta r_s \sim 1/nq'$ and the global scale a. We then may employ WKB asymptotic techniques to solve the complete 2-D problem [17–19]. It has been shown that the poloidal harmonics may be written in the form:

$$\delta\phi(r, m) = \mathcal{A}(\tau)\delta\phi(\tau, \tau - m), \quad (77)$$

where $\tau \equiv nq$ is a dimensionless radial "flux" coordinate. Equation (77) states that the form of the various poloidal harmonics is nearly translationally invariant, due to the slow equilibrium variations.

In Section 3, where we were interested in the local stability properties of TAM on a given flux surface, the τ dependencies in Eq. (77) were neglected, and only the $\tau - m$ dependence of the shape function $\delta\phi(\tau, \tau - m)$ was assumed, which describes the fast radial variation of the different poloidal harmonics on the $\Delta r_s \sim 1/nq'$ scale. In the present 2-D analysis, instead, the shape function slightly changes from one poloidal harmonic to the next, due to the slow equilibrium variations. These slow changes are accounted for through the dependence of $\delta\phi(\tau, \tau - m)$ on the slow radial coordinate τ [17–19]. Slow equilibrium changes may also cause an amplitude modulation of the coupled poloidal harmonics. This is described by the *radial envelope* function $\mathcal{A}(\tau)$.

Since $n \gg 1$, we may assume an eikonal representation for the envelope $\mathcal{A}(\tau) \sim \exp i\int^\tau \theta_k(\tau)\,d\tau$, where θ_k is the WKB phase [21,22], for which $\partial_\tau\theta_k/\theta_k \sim O(1/n)$. Furthermore, as in Section 3, we let

$$\delta\phi(\tau, \tau - m) = \int_{-\infty}^{\infty} \exp(-i(\tau - m)\theta)\delta\Phi(\tau, \theta)\,d\theta.$$

Note the slow τ-dependence of $\delta\Phi(\tau, \theta)$; i.e., $|\partial_\tau \ln \delta\Phi| \sim O(1/n)$. Thus,

$$\begin{aligned} k_r\delta\phi(r, m) = &-i\partial_r\delta\phi = -inq'\partial_\tau\delta\phi = nq'\mathcal{A}(\tau) \\ &\times \int_{-\infty}^{\infty} \exp(-i(\tau - m)\theta) \\ &\times [\theta_k - \theta + O(1/n)]\delta\Phi(\tau, \theta)\,d\theta. \end{aligned} \quad (78)$$

Equation (78) gives a direct physical interpretation of the eikonal θ_k as the change in the local radial wave vector $\Delta k_r = nq'\theta_k$. Furthermore, Eq. (78) illustrates how the solution of a fully 2-D equation may be reduced to two nested 1-D problems due to the $n \gg 1$ assumption [17, 18]. To the lowest order, i.e., on the $\Delta r_s \sim 1/nq'$ scale, we need to solve the local problem on a given magnetic flux surface (fixed τ!), which may be cast into the form of the SAW equation, Eq. (41), by simply substituting $s\theta \to s(\theta - \theta_k)$. The difference with respect to the local stability analysis of Section 3 is due to the fact that, here, θ_k (treated as a flux label) and other equilibrium parameters keep track of radial profile variations, considering the plasma as a truly dispersive medium. The solution of this new local problem, assuming homogeneous boundary conditions, leads to a local dispersion relation for TAM, which may be cast into the general form

$$F(\omega; \tau, \theta_k) = 0, \quad (79)$$

$F(\omega; \tau, \theta_k)$ being the local dispersion function. It has been recently shown that, for an (s, α) model equilibrium, the general form of the local dispersion function for TAM is given by [19]:

$$\begin{aligned} F(\omega; \tau, \theta_k) = Z_f[&F_1(1 + 2\delta U_{K,u}) \\ &+ F_2(2\delta T_{K,u} + \delta T_{K,T}) - F_3\delta T_{K,T}] \\ &+ 2G_f[F_2(1 + 2\delta U_{K,u}) - F_1(2\delta T_{K,u} + \delta T_{K,T})] \\ &+ 2(H_f\cos\theta_k + L_f\sin\theta_k) \\ &\times [F_3(1 + 2\delta U_{K,u}) - F_1\delta T_{K,T}]. \end{aligned} \quad (80)$$

Here,

$$\delta U_{K,u} = \frac{\pi^2}{4s}\frac{e^2}{mc^2}\frac{q^2R_0^2}{k_\chi^2}\left\langle \frac{\Omega_d^2 Q F_0}{\Delta(1 + \Delta^2)^{3/2}} \times \left[\frac{-i\omega_t/2}{\omega_t^2/4 - \omega^2} + \frac{i3\omega_t/2}{9\omega_t^2/4 - \omega^2}\right]\right\rangle, \quad (81)$$

has an interpretation similar to $\delta T_{K,u}$, Eq. (55), with the difference that it is vanishing for energetic particles distribution functions symmetric in $v_\parallel$; whereas Z_f, G_f, H_f, L_f are the same functions of (s, α, θ_k) defined in Ref. [18], where their numerical values were tabulated and their approximate analytical estimates were given. They account for the core plasma fluid response. Meanwhile, $F_1 = A(0)B(0)$, $2F_2 = B^2(0) - A^2(0)$ and $2F_3 = B^2(0) + A^2(0)$ are expressed in terms of the solutions of Eq. (44), evaluated at $\theta_1 = 0$, and they describe the coupling of TAM to KAW. Equation (80) embraces, in a non-perturbative way, equilibrium fluid and kinetic core-plasma effects as well as energetic particle dynamics with finite orbit widths. For this reason, it may be viewed as a unified description of TAE, KTAE and EPM. In the $s, \alpha < 1$ limit, Eq. (80) reduces to Eqs (57) and (64), since $Z_f \sim 1$, $G_f \sim s\pi/4$ and $H_f\cos\theta_k + L_f\sin\theta_k \sim G_f(\alpha/\alpha_c)$ [18].

Recalling Eq. (78), the SAW equation, Eq. (41), to the next order in the two spatial scale expansion, $O(1/n)$, i.e., on the characteristic equilibrium scales, becomes an equation for the radial envelope, $\mathcal{A}(\tau)$. This fact is readily recognized by recalling that $\theta_k = -i\partial_\tau \ln \mathcal{A}(\tau)$. It has been shown that the hence obtained WKB expression for $\mathcal{A}(\tau)$ is given by [17, 18]

$$\mathcal{A}(\tau) = \frac{K \exp\left(i\int^\tau \theta_k(\tau')\,d\tau'\right)}{\sqrt{(1/nq')\partial F/\partial\theta_k}}, \quad (82)$$

where K is an arbitrary constant and $F(\omega; \tau, \theta_k)$ is the local dispersion function. In Eq. (82), $\theta_k(\tau)$ is implicitly defined by the local dispersion relation, Eq. (79). The WKB expression for the mode envelope loses validity at the WKB turning-points (t.p.) positions, (τ_T, θ_{kT}), implicitly defined by the conditions $F(\omega; \tau_T, \theta_{kT}) = 0$ and $\partial_{\theta_k}F(\omega; \tau_T, \theta_{kT}) = 0$. In an up-down symmetric tokamak equilibrium, it may be shown that WKB t.p. are located at $\theta_{kT} = \ell\pi$, ℓ = integers. Furthermore, due to the 2π periodicity of the plasma equilibrium in the poloidal

direction, it is readily recognized that the real-θ_k space may be reduced to the first *Brillouin zone* $0 < \Re\theta_k < \pi$. When proper boundary conditions on the radial envelope function are applied, and the suitable *connection formulae* are used to analytically continue the WKB expression of $\mathcal{A}(\tau)$ through the existing t.p., the desired global mode structure and global dispersion relations are obtained [17–19]. It is therefore appropriate to say that all the information needed for a two-dimensional analysis of high-n modes is contained in the local dispersion function $F(\omega; \tau, \theta_k)$.

It is well known that, for an assigned global mode frequency, the WKB t.p. in the complex-τ plane are linked in "pairs" by the *anti-Stokes lines*, along which the WKB phase integral $\int_{\tau_T}^{\tau} \theta_k(\tau)\,d\tau$ is purely real. The Stokes structure of the complex-τ plane for TAM reflects the local TAM frequency spectrum, discussed in Section 4. In fact, recall that the local frequency spectrum is obtained from Eq. (80) for fixed τ and θ_k. Meanwhile, the WKB t.p. in the complex-τ plane are obtained from Eq. (80) for $\theta_k = 0$, π and ω fixed. Thus, the TAM Stokes plane shows one single TAE t.p. pair along with a sequence of more closely spaced KTAE t.p. pairs. For increasing core plasma pressure ($\alpha > \alpha_c$, cf. Section 4.A) the TAE pair merges into the KTAE t.p. sequence of the lower continuum, assuming the characteristics of a true KTAE t.p. pair; whereas, for sufficiently strong energetic particle drive, one particular KTAE t.p. pair emerges from the KTAE sequence and becomes clearly recognizable as that of an unstable EPM. In general, all existing WKB t.p. pairs must be taken into account. However, in the region of the τ-plane separating one t.p. pair to the next, the considered mode is *cut-off* (the radial envelope function $\mathcal{A}(\tau)$ is exponentially increasing/decreasing). Thus, in the $n \gg 1$ asymptotic limit, the coupling between separate t.p. pairs is exponentially small.

When t.p. coupling is neglected, it has been shown [17–19] that the global mode dispersion relation for a single t.p. pair, (τ_1, θ_{k1}) and (τ_2, θ_{k2}) with $\Re\tau_1 < \mathrm{Re}\,\tau_2$, reads

$$\epsilon_T\left(\int_{\tau_1}^{\tau_2} \hat{\theta}_k(\tau')\,d\tau' + \theta_{k1}\tau_1 - \theta_{k2}\tau_2\right) = (\mathcal{N} + w)\pi, \tag{83}$$

where $\epsilon_T = 1$ if $\theta_{k1} = 0$, $\epsilon_T = -1$ if $\theta_{k1} = \pi$, $\hat{\theta}_k$ is the branch of θ_k chosen such that $0 \le \Re\hat{\theta}_k \le \pi$, $\mathcal{N}$ is the radial mode number, and $w = 1/2$ (for $\theta_{k1} = \theta_{k2}$) or $w = 0$ (for $\theta_{k1} \neq \theta_{k2}$). The corresponding radial envelope function $\mathcal{A}(\tau)$ is given in Refs [17, 18].

Finite t.p. coupling accounts for non-local interactions of different TAM branches. A well known example of such non-local interactions is the coupling of TAE to KTAE. When the TAE growth rate is bigger than the typical frequency separation of KTAE, TAE modes see the kinetic spectrum as a continuum, i.e., the ideal SAW continuum. The non-local coupling of TAE to the SAW continuum requires the generalization of the *ballooning formalism* to handle the singular structures of the poloidal harmonics excited in the continuum. This issue is discussed in great detail in Refs [17, 18], where the perturbative calculation of the *continuum damping* due to small but finite coupling of TAE to the SAW continuum is presented. To solve this problem non-perturbatively, Eq. (83) needs to be generalized to include many coupled t.p. pairs.

Note that, according to Eq. (83), for each single t.p. pair there are many possible global mode frequencies, one for each radial mode number. The typical number of roots of the global dispersion relation, Eq. (83), scales as nq. Meanwhile, $|\tau_2 - \tau_1|$ is the characteristic number of coupled poloidal harmonics in which the global mode may be decomposed, as in Eq. (20). The validity of the WKB approach requires that $|\tau_2 - \tau_1| \gg 1$. In fact, the error on the WKB estimate of the global mode frequency, done with Eq. (83) is given by

$$\omega = \omega_{WKB}\left[1 + O(\epsilon_0) + O\left(\frac{1}{|\tau_2 - \tau_1|^2}\right)\right]. \tag{84}$$

Note that the $O(\epsilon_0)$ error in Eq. (84) is due to the $\epsilon_0 \ll 1$ assumption done in the derivation of Eq. (80), and is not related to the WKB analysis adopted here. When $|\tau_2 - \tau_1| \lesssim 1$, Eq. (83) is not valid, and local theories apply (cf. Sections 3 and 4). In this latest case, in fact, only two poloidal harmonics are locally coupled on a given magnetic flux surface and completely determine the mode dynamics.

Detailed analyses of global TAM spectra, based on Eq. (83), with the local dispersion function given by Eq. (80), are given in Refs [17–19]. Here, we summarize the most relevant results on radial mode extensions, obtained therein. For TAE, the mode localization is essentially determined by the radial dependence of the frequency gap in the SAW continuum. Specifically, its radial width is given by $|\tau_2 - \tau_1|_{TAE} \sim nqs\epsilon_0 L_A/r_0$ (i.e., $|\Delta r|_{TAE} \sim \epsilon_0 L_A$), with L_A the characteristic scale length of the Alfvén frequency. Also KTAE may have rather extended radial mode structures, although they remain less broad than TAE. Specifically, $|\tau_2 - \tau_1|_{KTAE} \sim nqs\Delta_K^{1/2}\epsilon_0 L_A/r_0$ (i.e., $|\Delta r|_{KTAE} \sim \Delta_K^{1/2}|\Delta r|_{TAE}$). Finally, the radial extent of EPM is determined by the spatial dependence of the fast particles drive and by the resonance condition between the mode characteristic frequency and the energetic particles, resulting in $|\tau_2 - \tau_1|_{EPM} \sim nqs(\gamma/\omega_r)\epsilon_0 L_A/r_0$ (i.e., $|\Delta r|_{EPM} \sim (\gamma/\omega_r)|\Delta r|_{TAE}$). These results, along with Eq. (84), can be used to determine whether the global dispersion relation, Eq. (83), is required for stability studies of TAM, or local analyses may be sufficient. It is important to emphasize that, contrary to usual practices, 2-D analyses, based on Eq. (83), may be necessary also for KTAE and EPM.

6. Summary and discussions

In the present article, we have reviewed some fundamental *linear* wave and stability properties of shear Alfvén waves in *nonuniform* plasmas in axisymmetric toroidal *geometries*. We have tried to demonstrate that, due to effects of plasma nonuniformities and magnetic field geometries, the physics associated with shear Alfvén waves becomes rather rich and complex. This richness and complexities are intrinsically related to the existence of both discrete and continuous spectra. More specifically, while nonuniformities are responsible for the continuous spectrum, the geometrical effects tend to introduce frequency gaps, within which discrete eigenmodes can exist. Furthermore, since the discrete and continuous spectra involve two disparate spatial scales, the existence of both spectra and the finite coupling between them dictates that the wave structures are of two scales. This two-scale property, on the other hand, offers the opportunity of deriving analytical dispersion relations via asymptotic matching analyses as well as formulating the two-dimensional global eigenvalue problem as two nested one-dimensional ones. This formulation can naturally include the effects of kinetic excitations via resonances with energetic particles (e.g., alphas) in toroidal plasmas such as tokamaks. Consequently, it is justified to say that, at this stage, it exists at

least solid conceptual foundations for analyzing linear properties of shear Alfvén waves in rather general plasma equilibria.

The remaining exciting challenges, we believe, are in the area of *nonlinear* physics of shear Alfvén waves and associated particle dynamics. The issues such as the nonlinear evolution of collective shear Alfvén instabilities and possible anomalous losses of alpha particles in deuterium-tritium tokamak fusion experiments are not only crucially important to the success of the controlled thermonuclear fusion research but also have cross-disciplinary implications to space plasma physics research. Theoretical studies of these issues are in the beginning stage, and we can look forward to exciting and very likely controversial results.

Acknowledgements

This work is supported in part by U.S. D.o.E. Grant No. DE-FG03-94ER54271 and N.S.F. Grant ATM-9396158.

References

1. Alfvén, H., Nature **150**, 405 (1942).
2. Chen, L. and Hasegawa, A., Phys. Fluids **17**, 1399 (1974).
   Hasegawa, A. and Chen, L., Phys. Rev. Lett. **32**, 454 (1974).
3. Grossman, W. and Tataronis, J., Z. Phys. **261**, 217 (1973).
4. Ionson, J. A., ApJ **254**, 318 (1978).
5. Rosenbluth, M. N. and Rutherford, P. H., Phys. Rev. Lett. **34**, 1428 (1975).
6. Chen, L., in "Theory of Fusion Plasmas" (Editors J. Vaclavik, F. Troyon and E. Sindoni) (Editrice Compositori, Bologna, 1988), p. 327.
7. Fu, G. Y. and Van Dam, J. W., Phys. Fluids B **1**, 1949 (1989).
8. Hasegawa, A. and Mima, K., J. Geophys. Res. **83**, 1117 (1978).
9. Hasegawa, A., J. Geophys. Res. **81**, 5083 (1976).
10. Grad, H., Phys. Today **22**, 34 (1969).
11. Hasegawa, A. and Chen, L., Phys. Rev. Lett. **35**, 370 (1975).
12. Hasegawa, A. and Chen, L., Phys. Fluids **19**, 1924 (1976).
13. Kieras, C. E. and Tataronis, J. A., J. Plasma Physics **28**, 395 (1982).
14. Cheng, C. Z., Chen, L. and Chance, M. S., Annals of Physics **161**, 21 (1985).
15. Mett, R. R. and Mahajan, S. M., Phys. Fluids B **4**, 2885 (1992).
    Candy, J. and Rosenbluth, M. N., Plasma Phys. Contr. Fus. **35**, 957 (1993).
16. Chen, L., Phys. Plasmas **1**, 1519 (1994).
17. Zonca, F. and Chen, L., Phys. Rev. Lett. **68**, 592 (1992).
18. Zonca, F. and Chen, L., Phys. Fluids B **5**, 3668 (1993).
19. Zonca, F. and Chen, L., Phys. Plasmas (1995) to be published.
20. Connor, J. W., Hastie, R. J. and Taylor, J. B., Proc. R. Soc. London Ser. A **365**, 1 (1979).
21. Dewar, R. L., Manickam, J., Grimm, R. C. and Chance, M. S., Nucl. Fusion **21**, 493 (1981).
22. Lee, Y. C. and Van Dam, J. W., in "Proceedings of the Finite Beta Theory Workshop, Varenna, 1977" (Editors B. Coppi and W. Sadowski) US D.o.E. CONF-7709167, p. 93.
23. Connor, J. W., Hastie, R. J. and Taylor, J. B., Phys. Rev. Lett. **40**, 396 (1978).
24. Tsai, S. T. and Chen, L., Phys. Fluids B **5**, 3284 (1993).
25. Gorelenkov, N. N. and Sharapov, S. E., Phys. Scr. **45**, 166 (1992).